Anomalous Reflection with Omnidirectional Active Metasurfaces Operating in Free Space

Yuxin Zhai[®],* Hyung-Suk Kwon[®], and Bogdan-Ioan Popa^{®†}
Department of Mechanical Engineering, University of Michigan, 48109, Ann Arbor, USA

(Received 12 February 2021; revised 3 August 2021; accepted 24 August 2021; published 13 September 2021)

Metasurfaces that manipulate the reflection of impinging sound have recently received significant attention, but virtually all past designs are passive structures with high temporal and spatial dispersion and thus have narrow bandwidths and are unidirectional. In this work, we introduce a method to design omnidirectional and broadband anomalous acoustic reflectors composed of nonresonant active scatterers arranged in a periodic lattice of subwavelength periodicity. The method relies on the manipulation of the wave-vector component parallel to the reflector's surface (i.e., transverse component) in a broadband manner and for arbitrary impinging sound directions. To illustrate our method experimentally, we design and measure an anomalous reflecting metasurface operating in free space for which the transverse wave-vector components of the incident and reflected waves differ by a prescribed constant. We show that the effect does not depend on the direction of incidence and has a bandwidth an order of magnitude larger than passive anomalous reflectors. This work shows that the active scatterers behave similarly to the atoms of a natural material rather than the unit cells of gratings or phononic crystals in that rearranging the active scatterers changes the metasurface geometry while preserving the device's desired functionality.

DOI: 10.1103/PhysRevApplied.16.034023

I. INTRODUCTION

Acoustic anomalous reflectors are structured surfaces that reflect impinging acoustic waves in tailored directions that do not obey Snell's law [1]. Research on controlling the acoustic reflection has received increasing interests in recent years due to its potential to improve acoustic wave control, such as achieving acoustic cloaking [2-5], acoustic nonreciprocity [6], and nontraditional acoustic lenses [7,8]. Traditionally, controlling the direction of the reflected waves is achieved through phase-gradient manipulation in metasurfaces [9-19], but this class of gradient metasurfaces are all passive, nontunable, and rely on resonators or long, coiled channels that impose a significant phase-shift dependency with frequency and thus reduce the operation bandwidth significantly. Furthermore, an acoustic anomalous reflector based on diffraction gratings was recently proposed [4,20-25] but these devices have high spatial dispersion and thus they manipulate the reflection in prescribed ways for very limited angles of incidence.

In this paper, we show that active acoustic metasurfaces address the limitations of previous passive solutions and enable broadband and omnidirectional anomalous reflectors. The work brings three major contributions. First, the proposed active metasurfaces control the direction of

the incoming wave by injecting energy into the system using active scatterers and does not rely on high spatial and temporal dispersion structures. As a result, the useful effect does not depend on the direction of incidence and is maintained in a significantly higher bandwidth than possible with passive devices. Second, we show through measurements done in a three-dimensional space that our metasurfaces behave like continuous materials in which the reflector shape can be changed by modifying the unitcell arrangements to fill the desired shape. This effect is a consequence of the subwavelength lattice periodicity, which means that the unit cells composing the metasurface behave like the atoms in a natural material rather than the unit cells of a grating or phononic crystal. Third, the reflectors' behavior is fully tunable their acoustic response being produced by active scatterers (meta-atoms) using the local sensor-driver architecture [26–31].

II. ACTIVE METASURFACE DESIGN

Figure 1(a) shows the basic behavior of a flat reflecting surface interacting with a plane wave of wave vector \bar{k}_i . If the reflector is large enough, the reflected field is typically dominated by a specular plane wave of wave vector \bar{k}_s so that the components of these wave vectors parallel to the surface (called transverse wave-vector components throughout the paper) are the same. Anomalous reflectors are able to break this fundamental boundary condition and modify the transverse wave-vector component and thus the

^{*}yxzhai@umich.edu

[†]bipopa@umich.edu, http://popa.engin.umich.edu/

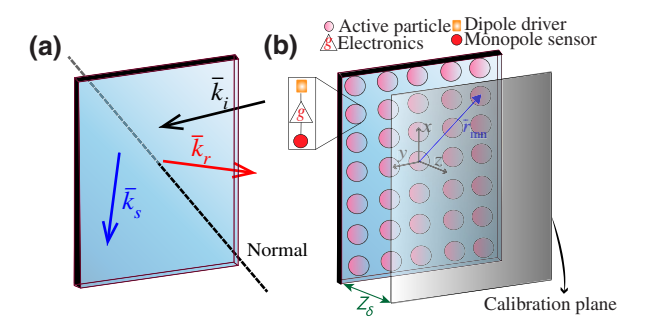


FIG. 1. Anomalous reflection. (a) A conventional smooth surface reflects an incident plane wave of wave vector \bar{k}_i in the specular direction \bar{k}_s . The aim is to redirect the reflected wave so that it has the nonspecular wave vector \bar{k}_r . (b) A metasurface is obtained by embedding active scatterers inside the smooth reflector. Each meta-atom contains a monopole sensor, a dipole-driven transducer and electronics to prescribe the impulse response between the sensor and the driver. The realized metasurface is calibrated by performing measurements on a plane situated at distance z_δ from the metasurface.

direction of the reflected wave (see \bar{k}_r in the figure). Here we obtain this behavior by leveraging on a matter model that describes any medium in terms of periodic arrangements of polarized scattering inclusions [27,28,32]. We implement an anomalous reflector by embedding active scatterers in a passive reflecting surface of reflection coefficient Q and we use the following approach to design the scatterers' polarizabilities so that they modify the transverse component of \bar{k}_r as desired. The polarized scatterer model defines four types of scattering inclusions differentiated based on whether they react to the monopole or dipole moment of the local acoustic field and whether the scatterers' local acoustic responses have nonzero monopole or dipole moments. The choice of inclusion type is important to minimize temporal dispersion and thus maximize bandwidth. Inclusions that respond to one type of multipole moment and generate the same type of moment (monopole-monopole or dipole-dipole) have the disadvantage of a feedbacklike response that depends strongly on frequency. This occurs because the inclusions respond not only to the external impinging field but also to the field scattered by itself [26]. From a practical point of view it is more advantageous to employ inclusions that respond to one multipole moment by producing the other. This assures that the scatterer does not react to its own scattered fields and therefore they are not as dispersive. The latter types of scatterers have recently been associated with Willis media [27,28,30,32].

In particular, in this work we employ inclusions that sense the monopole moment and respond by creating a dipole moment [27,28]. Consequently, each scattering inclusion senses the local pressure field p_I and produces

a scattered field whose acoustic pressure is given by

$$p(\bar{r}) = \alpha p_l \frac{e^{-jk_0|\bar{r}|}}{|\bar{r}|} \cos(\beta), \tag{1}$$

where the position vector \bar{r} defines the point where the scattered field is evaluated relative to the inclusion's position, α is the scatterer polarizability, $k_0 = \omega/c_0$ is the wave number, c_0 is the speed of sound, and β is the angle between \bar{r} and the normal to the reflector surface. In the above equation and throughout the paper, we assume harmonic fields of angular frequency ω and time dependency $e^{j\omega t}$.

The scattered field $p(\bar{r})$ vanishes on the reflector's surface because the angle $\beta=90^\circ$ for all points on this surface. Consequently, all inclusions are completely decoupled from each other, i.e., the sound scattered by any of them does not have any influence on its neighbors. This allows us to analytically compute the field reflected by the reflector. Assuming that the inclusions are placed on a uniform grid of periodicity d, as shown in Fig. 1(b), the reflected field can be written as the superposition between the specular reflection due to the passive surface, $p_s(\bar{r})$ and the contributions of the active scatterers given by Eq. (1). Specifically,

$$p_r(\bar{r}) = p_s(\bar{r}) + \sum_{n,m} \alpha_{mn} p_i(\bar{r}_{mn}) \frac{e^{-jk_0|\bar{r} - \bar{r}_{mn}|}}{|\bar{r} - \bar{r}_{mn}|} \cos(\beta_{mn}), \quad (2)$$

where m and n are integer indexes identifying the inclusions, $\bar{r}_{mn} = md\hat{x} + nd\hat{y}$ and α_{mn} are the position vector and polarizability of inclusion mn, and \hat{x} and \hat{y} are unit vectors defining the Cartesian coordinate system shown in Fig. 1(b). Equation (2) shows that we could achieve any value of p_r by carefully choosing the values of α_{mn} .

In the following we consider an incident plane wave of acoustic pressure $p_i(\bar{r}) = e^{-j\bar{k}_i \times \bar{r}}$ with $\bar{k}_i = k_0[-\sin(\theta)\hat{y} - \cos(\theta)\hat{z}]$, where θ is the incident angle with respect to normal to the reflector. Applying the Rayleigh-Sommerfeld diffraction formula used to compute (in the general case) how fields on an aperture propagate in the far field, the specular reflection at any point in space in the absence of the active scattering inclusions is

$$p_{s}(\bar{r}) = \iint_{A} Qp_{i}(\bar{r}') \frac{e^{-jk_{0}|\bar{r}-\bar{r}'|}}{|\bar{r}-\bar{r}'|} \cos(\beta) dx' dy'$$

$$= \iint_{A} Qe^{jk_{0}\sin(\theta)y'} \frac{e^{-jk_{0}|\bar{r}-\bar{r}'|}}{|\bar{r}-\bar{r}'|} \cos(\beta) dx' dy', \quad (3)$$

where the integral is over the surface A of the passive reflecting surface, the position vector $\vec{r}' = x'\hat{x} + y'\hat{y}$ indicates the position of any point on the surface of the reflector, and Q is the local reflection coefficient at the position of the unit surface dx'dy'. Per the Rayleigh-Sommerfeld

formula, the angle β represents the angle between the position vector r and the normal to the reflector.

When the reflector is large enough, the total reflected field is dominated by a single specular plane-wave component. Consequently, Eq. (3) can be approximated as $p_s(\bar{r}) \approx Q e^{-j\bar{k}_s \cdot \bar{r}}$, where $\bar{k}_s = k_0 [-\sin(\theta)\hat{y} + \cos(\theta)\hat{z}]$.

Our goal is to leverage the active scattering inclusions to change the direction of p_s by injecting a prescribed value $\bar{k}_a = k_x \hat{x} + k_y \hat{y}$ to the in-plane component of the reflected wave vector. In other words, we aim to engineer a reflected wave that has the following expression:

$$p_{r}(\bar{r}) = \iint_{A} Q e^{j[k_{0}\sin(\theta)y' + \bar{k}_{a}\times\bar{r}']} \frac{e^{-jk_{0}|\bar{r}-\bar{r}'|}}{|\bar{r}-\bar{r}'|} \cos(\beta) dx' dy'.$$
(4)

If the inclusion spacing d is significantly smaller than the in-plane wavelength $2\pi/[k_i\sin(\theta)]$ then the acoustic pressure gradient is small on any d by d patch on the reflector surface. Consequently, Eqs. (3) and (4) can be approximated as discrete sums

$$p_s(\bar{r}) \approx d^2 \sum_{n,m} Q e^{jk_0 \sin(\theta)nd} \frac{e^{-jk_0|\bar{r} - \bar{r}_{mn}|}}{|\bar{r} - \bar{r}_{mn}|} \cos(\beta_{mn})$$
 (5)

and, respectively,

$$p_r(\bar{r}) \approx d^2 \sum_{n,m} Q e^{j[k_0 \sin(\theta)nd + \bar{k}_a \times \bar{r}_{mn}]} \frac{e^{-jk_0|\bar{r} - \bar{r}_{mn}|}}{|\bar{r} - \bar{r}_{mn}|} \cos(\beta_{mn}).$$

$$(6)$$

In this work we choose d so that it is smaller than an eighth of the smallest in-plane incident wavelength. We show experimentally that this limit for d produces excellent results.

Plugging Eqs. (5) and (6) into Eq. (2), we identify the terms corresponding to the n and m indexes to determine the polarizabilities α_{mn} that enforce the desired anomalous reflected field p_r and obtain

$$\alpha_{mn} = d^2 Q e^{i(k_x md + k_y nd)} - d^2 Q. \tag{7}$$

The above equation provides the design polarizabilities α_{mn} needed to inject any desired in-plane wave-vector component \bar{k}_a . Each polarizability is written as the sum of two terms. The first contributes to the generation of the anomalous reflection and the second cancels the specular reflection from the passive reflector frame. Equation (7) also shows that the amplitude of the acoustic pressure scattered by each inclusion is inverse proportional to the number of inclusions, which implies that for less dense inclusion arrangements, the locally produced responses could be significantly larger than the local p_i . Hence,

the scatterers necessarily need to be active for broadband operation.

We illustrate this design procedure in experiments in which we aim to inject a wave-vector component parallel to the reflector surface of $\bar{k}_a = k_y \hat{y}$. As a result, the relationship between the incident (θ) and reflected (ϕ) angles becomes

$$\sin(\phi) = \sin(\theta) + \frac{k_y}{k_0}.$$
 (8)

We consider here the interesting case in which we choose k_y so that a normally incident wave ($\theta = 0^{\circ}$) is reflected at a significantly different angle $\phi = -60^{\circ}$. The above equation gives

$$k_{v} = -k_0 \sqrt{3}/2. (9)$$

We realize the active scattering inclusions for anomalous reflectors with Willis active meta-atoms. The meta-atoms are designed following the sensor-driver architecture [26] and used to obtain broadband unidirectional metasurfaces [27,28]. In this architecture each unit cell has an omnidirectional sensor implemented using two microphones attached to each side of the reflector. The electrical signals produced by the microphones are added in phase so that they measure the monopole moment of the local acoustic field. Similarly, unit cell has a dipole source created with two back-to-back speakers driven 180° out of phase and attached on the two sides of the reflector. The active dipole creates the field scattered by the active metaatom. The advantage of this approach lies in its acoustic properties being set entirely in the electronics connecting the sensing and driven transducers. This means that meta-atoms previously employed for different applications [27,28] could be repurposed by simply reprogramming the impulse responses of their microntroller-based electronic circuits. Each meta-atom's polarizability is controlled by judiciously choosing the amplitude and phase of the electronics impulse response g (see Fig. 1) to achieve the desired polarizabilities α_{mn} prescribed by Eq. (7). Since the design of the realized active meta-atom has been presented in detail elsewhere [27,28] we show the meta-atom design for this paper within the Supplemental Material [33] and we demonstrate how to select the electronics transfer function to realize omnidirectional anomalous reflectors. The main factor that limits the working bandwidth of the metasurface is the processing speed of the electronic components such as digital filters and analog amplifiers. Ideally, the phase of the transfer function of the electronic circuit between the sensor and driver should be constant. However, the delay caused by these electronic circuits introduce a phase that decreases with frequency and the slope of this phase versus frequency is dictated by the delay through the electronics. If the electronics are fast enough,

the slope will decrease and the working bandwidth will thus become larger.

III. EXPERIMENTAL VALIDATION

The photograph of the fabricated active Willis metaatom is shown in Fig. 2. The term "meta-atom" is justified here because the active unit cells behave like the building blocks of an effective artificial material that reflects sound in nonspecular directions. To prove this, we arrange the meta-atoms in two configurations that implement metasurface reflectors of the same acoustic properties but different geometrical shapes. The first metasurface is a square reflector made of 3×3 meta-atoms [see Fig. 2(a)] and the second is a rectangular reflector made of 6×1 meta-atoms [see Fig. 2(b)]. This behavior is fundamentally different from traditional active sound-control approaches in which replicating an active sound-control system does not yield a better system capable of manipulating sound in a larger space.

The calibration procedure that sets the meta-atom polarizabilities α_{mn} according to Eq. (7) and the metasurface performance are based on free-space measurements performed with the experimental setup shown in Fig. 2(c). A speaker placed 50-cm away ensonifies the reflector with short Gaussian pulses five periods long at the center frequency of 2400 Hz. The acoustic fields are measured on a plane in front of the reflector under test by raster scanning the surface of the plane with a microphone. Figure 2(d) shows the measured incident fields $p_i(\bar{r})$ produced by the source speaker for two speaker positions, namely for normal and 30° angle of incidence. In the following, all angles

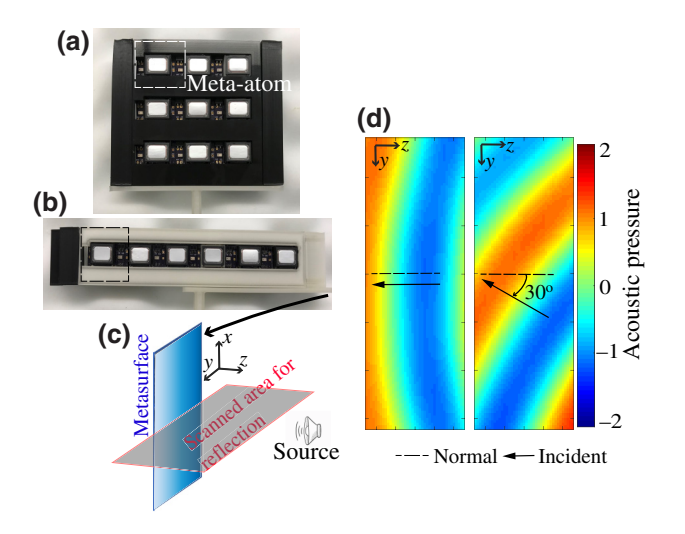


FIG. 2. Experimental setup. Two metasurface configurations having (a) 3×3 meta-atoms and (b) 6×1 meta-atoms are measured. (c) The metasurface behavior is quantified through measurements along the *y-z* plane perpendicular to the metasurface. (d) The acoustic incident fields are measured for normal (left) and 30° (right) incidence at 2400 Hz.

are measured relative to the z axis perpendicular to the reflector.

Even though Eq. (7) defines the meta-atom polarizabilities α_{mn} unambiguously, using this equation directly is difficult because Q depends on the impulse response between the meta-atom sensing and driven transducers and thus depends on the impulse responses of these transducers, which are more difficult to measure accurately. Instead, we use the following approach based on Eq. (2). For calibration purposes we use the 3×3 meta-atom reflector of Fig. 2. For this reflector we measure the specular reflection for normal incidence by inactivating all inclusions, i.e., by turning off the active response of the metasurface and thus setting $\alpha_{mn} = 0$. The specular reflection is $p_s(\bar{r}) = p_r(\bar{r})$ – $p_i(\bar{r})$, where p_r and p_i are the total acoustic pressure fields measured with and without the inactivated metasurface. Then we optimize each meta-atom individually by turning on the meta-atoms one at a time while keeping the rest inactivated and modify the electronics impulse response g [see Fig. 1(b)] of the selected meta-atom to minimize the total acoustic pressure at an acoustically small distance $z_{\delta} = 5$ mm in front of the activated meta-atoms. The points where we minimize the total acoustic pressure will thus lie in a plane situated z_{δ} away from the metasurface and labeled "calibration plane" in Fig. 1(b). By minimizing p_r in front of the activated meta-atom we essentially find the impulse response g_0 providing the -Qd term of Eq. (7), which cancels the reflected wave altogether. This procedure works as long as z_{δ} is small enough so that $p_r(\bar{r}_{mn} + z_{\delta}\hat{z})$ is dominated by the active field produced by the meta-atom positioned at \bar{r}_{mn} .

Once we have the experimentally derived g_0 , we realize α_{mn} of Eq. (7) by using the following impulse response g_{mn} for the meta-atom identified by the pair (m, n)

$$g_{mn} = -g_0 e^{jk_y nd} + g_0. (10)$$

It is important to note that the value of Q, the local reflection coefficient of the passive reflector, does not depend on the direction of incidence or the details of the impinging external field. This is in stark contrast with traditional active sound control, which requires sampling the incident field and dynamically modifying the impulse responses between sensing and driven transducers. There are two remarkable consequences of this.

First, even though the value of Q has been found for normal incidence, the metasurfaces implementing these values of Q will work for any impinging wave. This is demonstrated in the measurements shown within the Supplemental Material [33]. Second, the value of Q is set in a predetermined way for a given application and therefore can be realized with very simple electronics that need only to impose a fixed phase and amplitude values for α_{mn} that do not depend on the incoming sound. Therefore, the

bandwidth of the metasurface can be significantly larger than possible in traditional active sound-control systems.

IV. EXPERIMENTAL RESULTS

Figures 3(a) and 3(b) show the performance of the metasurface composed of 3×3 meta-atoms compared against numerical simulation of an ideal anomalous reflector that modifies the transverse wave-vector component by a factor k_y given by Eq. (9). Figure 3(a) shows side by side the specular reflection to a normally incident acoustic field obtained with the meta-atoms turned off. As expected the plane-wave decomposition of the reflected acoustic wave is dominated by a component whose associated wave vector is perpendicular to the metasurface.

Upon activating the meta-atoms, the reflected wave changes its direction by 60° as predicted by Eq. (8) (see the middle panel) and, remarkably, the specular component completely disappears. The excellent performance of the metasurface is further confirmed by comparing the measured reflection with the reflection from an ideal anomalous reflector that injects a transverse wave-vector component $\bar{k}_a = k_y \hat{y}$, where k_y is given by Eq. (9). The numerical simulation that produces the fields scattered by the ideal anomalous reflector is carried out in MAT-LAB using the following approach. The specular reflections measured in the experiment with the inactivated metasurface are decomposed into plane waves and their wavevector components parallel to the metasurafce are modified by the constant value \bar{k}_a . The resulting reflected wave fronts are propagated using Green's function method.

A remarkable property of the active anomalous reflector that sets it apart from its passive counterparts reported previously [4,20,21,23,24] is its omnidirectionality, i.e., its ability to function as designed for a large range of angles of incidence. To illustrate this property, we changed the angle of incidence to $\theta = 30^{\circ}$. Equation (8), predicts an nonspecular reflection angle $\phi = -21^{\circ}$, which corrsponds

to a negatively reflected wave propagating back towards the source. Figure 3(b) shows the excellent match between the ideal and measured field in this case as well, which demonstrates the metasurface omnidirectional nature.

More importantly, there is nothing special about the shape of the metasurface used to obtain the experimental results shown in Figs. 3(a) and 3(b). The meta-atoms composing the metasurface can be rearranged in other configurations to realize different metasurface geometries that maintain the initially prescribed anomalous reflection behavior. We demonstrate this remarkable property in an experiment involving a metasurface composed of a linear array of 6×1 meta-atoms. The acoustic strength of the meta-atom acoustic response is kept unchanged because the constant g_0 in Eq. (10) does not depend on the meta-surface configuration, but the phase delay between adjacent meta-atoms dictated by the ejkynd term is modified to realize the impulse responses required by Eq. (10). The experimental results involving the reshaped metasurface shown in Fig. 2(b) are presented in Figs. 3(c) and 3(d). The measured reflections match very well the expected ideal behavior for multiple angles of incidence ($\theta = 0^{\circ}$ and $\theta = 30^{\circ}$ are shown in the figure) and demonstrate that the anomalous reflection behavior of the metasurfaces, including their negative reflection ability, is preserved upon rearranging the meta-atoms.

To demonstrate the bandwidth capability of our metasurfaces we show in Fig. 4 the reflected far field for the $\theta=0^\circ$ and $\theta=30^\circ$ angles of incidence for various frequencies. In all situations the measurements (solid lines) matched very well the simulated, ideal behavior (dashed lines), which demonstrates the broadband behavior of the metasurfaces. The specular directions are shown in the figure and highlight the flexibility afforded by anomalous reflectors realized with active metasurfaces. The results show that the desired functionality occurs in a large bandwidth of at least 8% around the central frequency of 2400 Hz and for angles of incidence covering a large solid angle. This

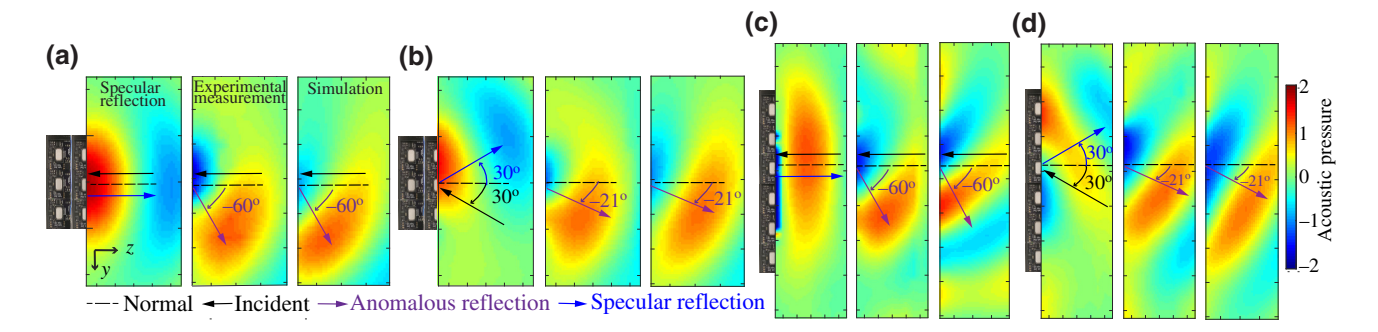


FIG. 3. Experimental results at 2400 Hz. (a) The acoustic response of the first metasurface made of 3×3 meta-atoms to a normally incident spherical wave. The specular reflection obtained with the deactivated meta-atoms (left) is compared against the anomalous reflection obtained with the activated meta-atoms (center) and the expected, prescribed nonspecular reflection obtained in numerical simulations. (b) The same measurements as in (a) performed for 30° incidence. (c),(d) Same measurements as in (a),(b) for the second metasurface composed of 6×1 meta-atoms.

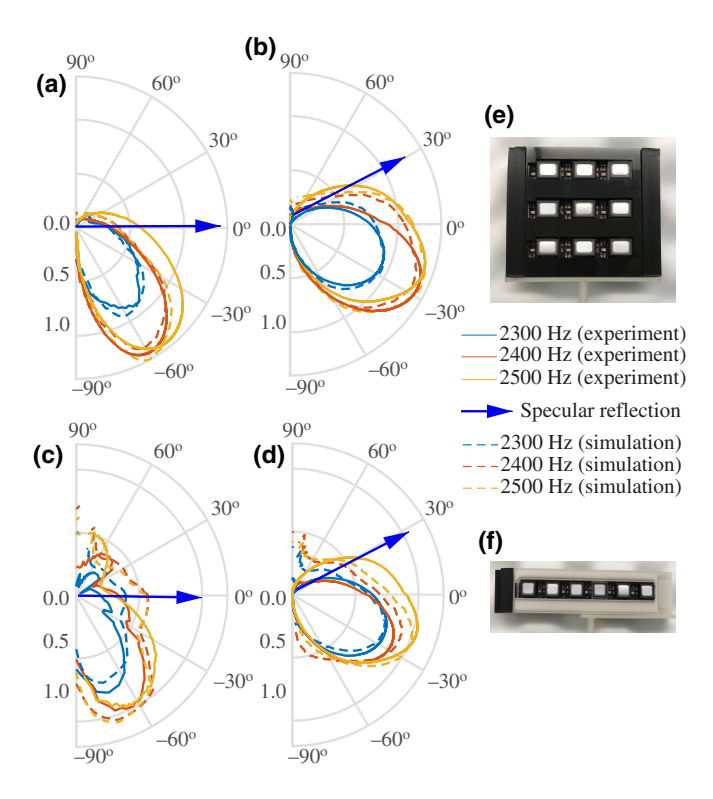


FIG. 4. Far-field acoustic pressure amplitude of the reflected wave. The reflections [(a),(b)] and [(c),(d)] are from the metasurfaces composed of 3×3 meta-atoms (e) and 6×1 meta-atoms (f), respectively. The reflections are shown when the incident angles are [(a),(c)] 0° and [(b),(d)] 30° . For each case, the measured (solid line) and simulated (dashed line) reflection are shown for at 2300, 2400, and 2500 Hz.

is in contrast with passive anomalous reflectors reported so far, which were either unidirectional or had bandwidths significantly below 1%.

V. CONCLUSION

To conclude, we show that active metasurfaces address two fundamental limitations of passive anomalous reflectors. Passive structures that do not obey Snell's law must have strong spatial and temporal dispersion and therefore operate in prescribed ways for one direction of incidence and have a very narrow bandwidth. We show theoretically and experimentally that active metasurfaces realized with meta-atoms based on the sensor-driver architecture address these limitations. The meta-atoms are selfcontained, individual material building blocks that can be arranged like Lego pieces to implement any metasurface geometry desired. The design equations derived in the paper are demonstrated experimentally in threedimensional experiments for two metasurface configurations. Even though we present one example of anomalous reflector, which rotates the reflection direction by approximately 60° from its specular direction, the metasurface could be programmed to realize a wide range of functionalities by changes in the meta-atom impulse response between its sensor and driver. We thus believe that the approach presented here will broaden the avenues for sound propagation control.

ACKNOWLEDGMENTS

This material is based upon work supported by the National Science Foundation under Grant No. CMMI-1942901.

- L. E. Kinsler, A. R. Frey, A. B. Coppens, and J. V. Sanders, Fundamentals of Acoustics (John Wiley & Sons, Hoboken, New Jersey, 1999).
- [2] B.-I. Popa, L. Zigoneanu, and S. A. Cummer, Experimental Acoustic Ground Cloak in Air, Phys. Rev. Lett. 106, 253901 (2011).
- [3] C. Faure, O. Richoux, S. Félix, and V. Pagneux, Experiments on metasurface carpet cloaking for audible acoustics, Appl. Phys. Lett. **108**, 064103 (2016).
- [4] Y. Jin, X. Fang, Y. Li, and D. Torrent, Engineered Diffraction Gratings for Acoustic Cloaking, Phys. Rev. Appl. 11, 011004 (2019).
- [5] H. Esfahlani, S. Karkar, H. Lissek, and J. R. Mosig, Acoustic carpet cloak based on an ultrathin metasurface, Phys. Rev. B 94, 014302 (2016).
- [6] B. Liang, X. Guo, J. Tu, D. Zhang, and J. Cheng, An acoustic rectifier, Nat. Mater. 9, 989 (2010).
- [7] Y. Xie, W. Wang, H. Chen, A. Konneker, B.-I. Popa, and S. A. Cummer, Wavefront modulation and subwavelength diffractive acoustics with an acoustic metasurface, Nat. Commun. 5, 5553 (2014).
- [8] J. Li, C. Shen, A. Díaz-Rubio, S. A. Tretyakov, and S. A. Cummer, Systematic design and experimental demonstration of bianisotropic metasurfaces for scattering-free manipulation of acoustic wavefronts, Nat. Commun. 9, 1342 (2018).
- [9] J. Zhao, B. Li, Z. Chen, and C.-W. Qiu, Manipulating acoustic wavefront by inhomogeneous impedance and steerable extraordinary reflection, Sci. Rep. 3, 2537 (2013).
- [10] Y. Xie, A. Konneker, B.-I. Popa, and S. A. Cummer, Tapered labyrinthine acoustic metamaterials for broadband impedance matching, Appl. Phys. Lett. 103, 201906 (2013).
- [11] Y. Li, X. Jiang, R.-Q. Li, B. Liang, X.-Y. Zou, L.-L. Yin, and J.-C. Cheng, Experimental Realization of Full Control of Reflected Waves with Subwavelength Acoustic Metasurfaces, Phys. Rev. Appl. 2, 064002 (2014).
- [12] K. Tang, C. Qiu, M. Ke, J. Lu, Y. Ye, and Z. Liu, Anomalous refraction of airborne sound through ultrathin meta-surfaces, Sci. Rep. 4, 6517 (2014).
- [13] J. Mei and Y. Wu, Controllable transmission and total reflection through an impedance-matched acoustic metasurface, New J. Phys. **16**, 123007 (2014).
- [14] Y.-F. Zhu, X.-Y. Zou, R.-Q. Li, X. Jiang, J. Tu, B. Liang, and J.-C. Cheng, Dispersionless manipulation of reflected

- acoustic wavefront by subwavelength corrugated surface, Sci. Rep. **5**, 10966 (2015).
- [15] Y. Li, X. Jiang, B. Liang, J.-C. Cheng, and L. Zhang, Metascreen-Based Acoustic Passive Phased Array, Phys. Rev. Appl. 4, 024003 (2015).
- [16] W. Wang, Y. Xie, B.-I. Popa, and S. A. Cummer, Sub-wavelength diffractive acoustics and wavefront manipulation with a reflective acoustic metasurface, J. Appl. Phys. 120, 195103 (2016).
- [17] Y. Li, S. Qi, and M. B. Assouar, Theory of metascreenbased acoustic passive phased array, New J. Phys. 18, 043024 (2016).
- [18] Y. Zhang, B. Xie, W. Liu, H. Cheng, S. Chen, and J. Tian, Anomalous reflection and vortex beam generation by multibit coding acoustic metasurfaces, Appl. Phys. Lett. 114, 091905 (2019).
- [19] Y. Zhu, X. Zou, R. Li, X. Jiang, J. Tu, B. Liang, and J. Cheng, Dispersionless manipulation of reflected acoustic wavefront by subwavelength corrugated surface, Sci. Rep. 5, 10966 (2015).
- [20] L. Quan and A. Alù, Passive Acoustic Metasurface with Unitary Reflection Based on Nonlocality, Phys. Rev. Appl. 11, 054077 (2019).
- [21] D. Torrent, Acoustic anomalous reflectors based on diffraction grating engineering, Phys. Rev. B 98, 060101 (2018).
- [22] S. Qi and B. Assouar, Ultrathin acoustic metasurfacesfor reflective wave focusing, J. Appl. Phys. 123, 234501 (2018).
- [23] S. R. Craig, X. Su, A. Norris, and C. Shi, Experimental Realization of Acoustic Bianisotropic Gratings, Phys. Rev. Appl. 11, 061002 (2019).

- [24] H. Ni, X. Fang, Z. Hou, Y. Li, and B. Assouar, Highefficiency anomalous splitter by acoustic meta-grating, Phys. Rev. B 100, 104104 (2019).
- [25] S.-W. Fan, S.-D. Zhao, A.-L. Chen, Y.-F. Wang, B. Assouar, and Y.-S. Wang, Tunable Broadband Reflective Acoustic Metasurface, Phys. Rev. Appl. 11, 044038 (2019).
- [26] B.-I. Popa, L. Zigoneanu, and S. A. Cummer, Tunable active acoustic metamaterials, Phys. Rev. B **88**, 024303 (2013).
- [27] B.-I. Popa, Y. Zhai, and H.-S. Kwon, Broadband sound barriers with bianisotropic metasurfaces, Nat. Commun. 9, 5299 (2018).
- [28] Y. Zhai, H.-S. Kwon, and B.-I. Popa, Active Willis metamaterials for ultracompact nonreciprocal linear acoustic devices, Phys. Rev. B 99, 220301 (2019).
- [29] A. Baz, Active nonreciprocal metamaterial using an eigenstructure assignment control strategy, J. Acoust. Soc. Am. 147, 2656 (2020).
- [30] Z. Tian, C. Shen, J. Li, E. Reit, H. Bachman, J. E. Socolar, S. A. Cummer, and T. J. Huang, Dispersion tuning and route reconfiguration of acoustic waves in valley topological phononic crystals, Nat. Commun. 11, 762 (2020).
- [31] C. Cho, X. Wen, N. Park, and J. Li, Digitally virtualized atoms for acoustic metamaterials, Nat. Commun. 11, 251 (2020).
- [32] C. F. Sieck, A. Alù, and M. R. Haberman, Origins of Willis coupling and acoustic bianisotropy in acoustic metamaterials through source-driven homogenization, Phys. Rev. B **96**, 104303 (2017).
- [33] See Supplemental Material at http://link.aps.org/supplemental/10.1103/PhysRevApplied.16.034023 for a detailed description of the experimental results.